# PREPARATION OF A Cu-BTC/PAN ELECTROSPUN FILM WITH A GOOD AIR FILTRATION PERFORMANCE

by

***Cheng-Fei YANG[a], Dan TIAN[b], and Ji-Huan HE[a,b,c*]***

[a] National Engineering Laboratory for Modern Silk, College of Textile and Engineering, Soochow University, Suzhou, China
[b] School of Science, Xi'an University of Architecture and Technology, Xi'an, China
[c] School of Mathematics and Information Science, Henan Polytechnic University, Jiaozuo, China

Original scientific paper
https://doi.org/10.2298/TSCI200201048Y

*Copper-1,3,5-benzoic acid (Cu-BTC) was synthesized by the hydrothermal method, which had regular octahedral morphology. The Cu-BTC particles were used as additives in the polyacrylonitrile (PAN) solution fabricate Cu-BTC/PAN membrane by the electrostatic spinning method, its good filtration performance was witnessed experimentally.*

Key words*: metal organic framework, hydrothermal method, electrospinning, air filtration*

## Introduction

With the continuous development of science and technology and modern industry, environmental pollution has become one of the most serious problems facing mankind. When the content of PM2.5 is too high, human health will face a huge threat and even cause death [1]. People are paying more and more attention environmental air quality. The continuous development and improvement of dust removal and purification technology and the expansion of its application range have put forward new requirements on the quantity, variety and quality of air filter materials [2, 3]. In order to improve people's quality of life, air filter materials have become a research hotspot. How to reduce the harm of air pollution human health and life has become a major problem that needs to be solved urgently, and low dimensional materials are now widely used for this purpose.

Low dimensional materials, such as graphene [4, 5], nanofibers [6-14], and nanoparticles [15-20], have been widely used in many fields and have received much attention in recent years. Metal-organic framework (MOF) is a kind of new hybrid materials, which can be a 1-D, 2-D or 3-D structure consisting of rigid organic ligands and metal ions. Hoskins and Robson [21] first proposed the concept of MOF materials. He pointed out that the use of organic ligands and metal ions through co-ordination bonds can form a MOF material with a network structure. Because of its diverse and beautiful surface morphology, regular pore structure, large specific surface area, and coordination unsaturated metal vacancy, it has been widely used in traditional fields such as gas storage, separation, catalysis [22, 23], biomedical, sensor material [24] and other new fields. In recent years, people have compounded MOF with silica, titanium dioxide [25], graphene [26] and other materials to expand their performance and application fields.

* Corresponding author, e-mail: hejihuan@suda.edu.cn

The Cu-BTC was initially synthesized by Choi *et al*. [27] of Hong Kong University of Science and Technology by a hot solvent method and named as HKUST-1. The specific surface area is up to 1500 $m^2/g$, the pore structure is regularly arranged, and the chemical properties are stable. Among them, the metal clusters $Cu_2C_4O_8$ are interconnected to form a 3-D pore structure with a pore size of about 1 nm [28]. The central $Cu^{2+}$ in its skeleton structure adopts six co-ordination, 3 $Cu^{2+}$ are co-ordinated in space structure with 12 oxygen atoms on six carboxyl groups from two organic ligands BTC, and axially connected with two $H_2O$ co-ordination. After high temperature heating treatment, there appear metal vacancies with unsaturated co-ordination, which is conducive to the adsorption of small gas molecules. These unique advantages make Cu-BTC widely used in gas storage, separation, sensing, catalysis and other fields. The $SiO_2$-Cu-BTC can be used for the catalytic oxidation of active methylene compounds to obtain high yield and selectivity. In recent years, nanofibers prepared by electrospinning have been widely used. The modified nanofibers prepared by combining with organometallic framework materials have excellent properties [29-34]. The Cu-BTC/PVA film was prepared by electrospinning with the addition of Cu-BTC particles in PVA solution. The prepared Cu-BTC/PVA film has good bactericidal effect [35-37] and extremely excellent air filtration performance.

## Experimental design

The Cu-BTC particles were synthesized by the hydrothermal method. Dissolve 1.087 g $Cu(NO_3)2{\cdot}3H_2O$ in 15 ml deionized water, then dissolve 0.525g benzoic acid ($H_3$-BTC) in 15 ml anhydrous ethanol ($C_2H_5OH$), stir them evenly, transfer them to polytetrafluoroethylene reactor, and react for 12 hours at 120 °C. After the reaction, take out the polytetrafluoroethylene reaction kettle and cool it to room temperature in the drying oven. The reaction mixture was transferred to a centrifuge tube, using dimethylformamide (DMF) and absolute ethanol as detergents, and centrifuge at 9000 rpm for 10 minutes. After repeating the aforemenentioned operation three times, the resulting precipitate was placed in an 80 °C drying oven for 12 hours to obtain dark blue Cu-BTC particles.

The Cu-BTC/PAN film was prepared by electrospinning. 1.2 g PAN was added to 8.8 g DMF, after magnetic stirring for four hours, the mixed solution became a clear solution. The parameters of the electrospinning machine are set as: voltage 15 kV, flow rate 0.5 ml/h, reaction distance 15 cm. After spinning for 12 hours, a PAN film was obtained. With the same parameters, a clear solution with 12% PAN was prepared, and 0.2 g Cu-BTC particles were added. After stirring for 1 hour, the mixed solution of Cu-BTC/PAN was obtained. The Cu-BTC/PAN films were prepared by electrospinning with the same experimental parameters.

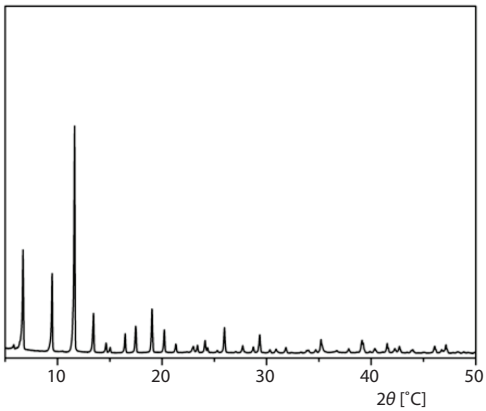


**Figure 1. The XRD pattern of Cu-BTC particles**

## Experimental analysis

Figure 1 is the XRD diagram of Cu-BTC particles, in which 6.7°, 9.6°, 11.7°, 13.5°, 14.7°, 15.1°, 16.6°, 17.5°, 19.1°, and 20.3° are the characteristic peaks of Cu-BTC, corresponding to (111), (200), (220), (222), (400), (331), (422), (333), (440), and (442) crystal faces of Cu-BTC, respectively. In line with the peak position in [30], the peak shape of XRD is sharp, indicating that the synthesized Cu-BTC crystal structure is

good. The Cu-BTC prepared by the hydrothermal method did not show the impurity peak of $2\theta = 11.0°$ reported in the XRD spectrum [38], indicating that the synthesis temperature was suitable and no CuO impurity was generated. The synthesized Cu-BTC particles are relatively pure and the structure is complete.

Figure 2 is the FT-IR spectrum of the sample Cu-BTC. It can be seen from the figure that two absorption peaks appear at 3458.1 $cm^{-1}$ and 1648.1 $cm^{-1}$, respectively, indicating that there is a certain amount of moisture in the synthesized sample. The absorption peaks at 1437 $cm^{-1}$ and 1369.4 $cm^{-1}$ are the asymmetric stretching vibration and symmetric stretching vibration absorption peaks of carbonyl in carboxyl group, respectively. The weak absorption peak at 956.3 $cm^{-1}$ is the stretching vibration absorption peak of C-O-Cu. The characteristic absorption peaks of Cu-BTC are 752.6 $cm^{-1}$ and 725.3 $cm^{-1}$, which are due to the substitution of groups on benzene ring by Cu. Compared with the literature [39], it can be seen that the peak position is consistent with the report.

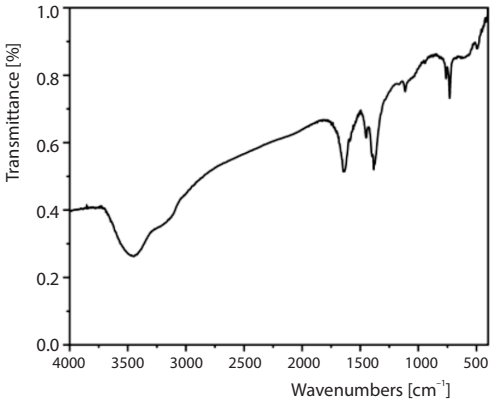


**Figure 2. The FT-IR pattern of Cu-BTC particles**

Figure 3 is a TGA graph of Cu-BTC particles. The Cu-BTC has three weightlessness intervals. During 50~180℃, the solvent molecules (ethanol and water) were volatilized, and the mass loss was about 29.2%; during 180~330 ℃ a continuous weight reduction process, about 6.1%, was mainly due to the removal of water molecules adsorbed on the $Cu^{2+}$ co-ordination bond in the Cu-BTC sample. When the temperature is over 330 ℃, there is an obvious weight loss range, and the mass loss drops sharply, indicating the decomposition of organic ligands. The crystal structure of Cu-BTC particles collapsed and decomposed completely at about 400 ℃, with 33.2% of the mass remaining. The decomposition product is CuO.

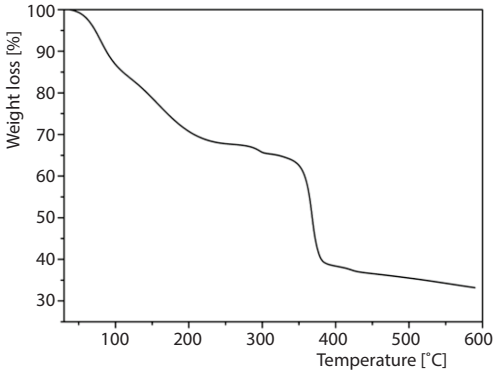


**Figure 3. The TGA pattern of Cu-BTC particles**

As shown in figs. 4(a) and 4(b) are SEM images of Cu-BTC particles. It can be clearly seen from the picture that a large number of regular octahedral crystals have been synthesized, which conforms to the crystal morphology of Cu-BTC particles described in the literature. At the same time, the crystal shape is complete and the surface is regular, showing a regular triangle surface. Figures 4(c) and 4 (d) are SEM of pure PAN film, and figs. 4(e) and 4(f) are SEM images of Cu-BTC/PAN film. By comparison, it can be seen clearly that the surface of the Cu-BTC/PAN film is smoother and the film is more uniform.

Tables 1-3 are the element distribution of Cu-BTC particles, PAN film, and Cu-BTC/PAN film, respectively. It can be found from tab. 1 that Cu-BTC particles are composed of carbon, oxygen, and copper. Among them, the content of carbon is the most, and the content of copper is the lowest. In tab. 2, there are only two elements in the PAN film,

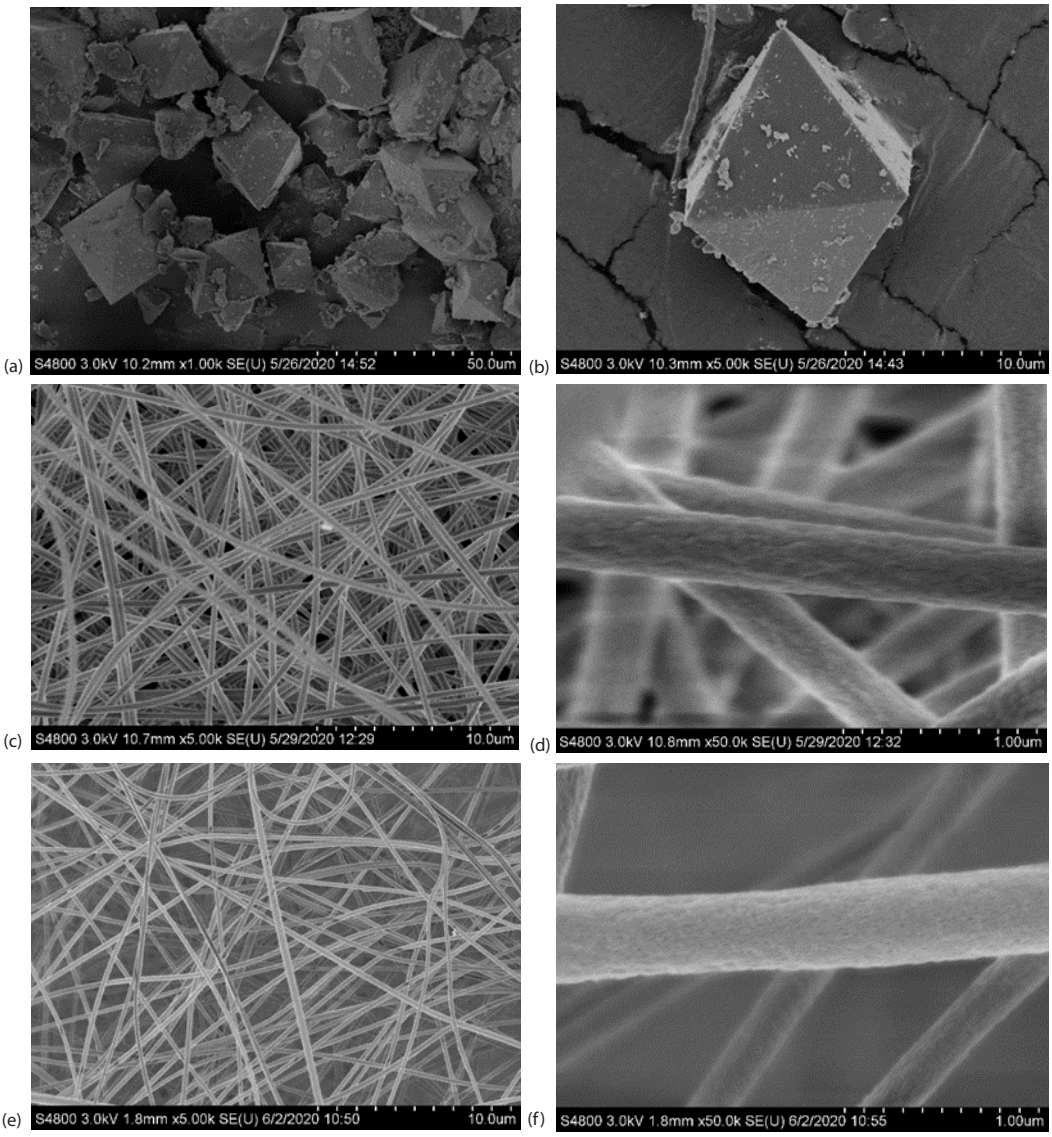


**Figure 4. (a) and (b) are SEM images of Cu-BTC particles, (c) and (d) are SEM images of PAN film, (e) and (f) are SEM images of Cu-BTC/PAN film**

namely carbon and nitrogen. At the same time, the content of carbon is about three times that of nitrogen. Observing the data in tab. 3, combined with tabs. 1 and 2, it can be found that the surface elements of the Cu-BTC/PAN film include all elements of the Cu-BTC particles and the PAN film. At the same time, the surface element content of Cu-BTC/PAN film conforms to the mass of Cu-BTC particles accounting for 2% of the Cu-BTC/PAN mixed solution. It shows that in the Cu-BTC/PAN film, the Cu-BTC particles are evenly distributed.

Generally speaking, the dispersed oil particulate (DOP) method is usually used to test the filtration performance of fiber membranes. The DOP method is also a common method for evaluating the gas permeability and resistance of the filter. Considering the practical application

**Table 1. The EDS test results of Cu-BTC particles**

| Element | Weight [%] | Atomic [%] |
|---|---|---|
| Carbon | 51.328 | 67.285 |
| Oxygen | 28.050 | 27.605 |
| Copper | 20.621 | 5.110 |

**Table 2. The EDS test results of PAN membrane**

| Element | Weight [%] | Atomic [%] |
|---|---|---|
| Carbon | 73.294 | 76.194 |
| Nitrogen | 26.706 | 23.806 |

**Table 3. The EDS test results of Cu-BTC/PAN membrane**

| Element | Weight [%] | Atomic [%] |
|---|---|---|
| Carbon | 67.902 | 71.752 |
| Nitrogen | 26.396 | 23.918 |
| Oxygen | 5.376 | 4.265 |
| Copper | 0.327 | 0.065 |

of nanofiber membranes, a parameter needs to be introduced to make a relatively balanced assessment between the filtration efficiency of the filter media and the pressure loss. Based on the filtration efficiency and pressure loss of the PAN membrane and Cu-BTC/PAN membrane, a quality factor is introduced as an evaluation parameter, which represents the relative ratio between the filtration efficiency and pressure loss of the same test sample, which is defined:

$$Q_F = \frac{-\ln(1-E)}{\Delta_P} \tag{1}$$

where $Q_F$ [Pa$^{-1}$] is the quality factor of the filtration performance evaluation of the fiber membrane, $E$ – [%] the filtration efficiency of fiber membrane, $\Delta P$ [Pa] – the pressure loss of fiber membrane.

It can be seen from eq. (1) that a higher $Q_F$ value means that the fiber filter membrane has better filtration performance. The air filtration performance of PAN membrane and Cu-BTC/PAN membrane is shown in tabs. 4 and 5. The average quality factor of PAN membrane filtration performance evaluation is only 0.0016 Pa$^{-1}$. The quality factor of Cu-BTC/PAN membrane filtration performance evaluation is 0.0135 Pa$^{-1}$ on average, about 8.5 times of PAN membrane. It can be explained that the air filtration performance of Cu-BTC/PAN membranes prepared by modifying PAN with Cu-BTC particles has been greatly improved compared to PAN membranes.

**Table 4. Results of DOP method test for PAN membrane**

| PAN | $E$ [%] | $\Delta P$ [Pa] | $Q_F$ [Pa$^{-1}$] |
|---|---|---|---|
| | 87.421 | 1488.3 | 0.0014 |
| | 89.159 | 1368.4 | 0.0016 |
| | 89.527 | 1393.7 | 0.0016 |
| | 91.482 | 1402.9 | 0.0018 |
| AVG | 89.397 | 1413.3 | 0.0016 |

**Table 5. The DOP test results of Cu-BTC/PAN membrane**

| Cu-BTC/PAN | $E$ [%] | $\Delta P$ [Pa] | $Q_F$ [Pa$^{-1}$] |
|---|---|---|---|
| | 99.994 | 762.4 | 0.0128 |
| | 99.999 | 602.1 | 0.0191 |
| | 99.996 | 767.6 | 0.0132 |
| | 99.992 | 803.1 | 0.0118 |
| AVG | 99.995 | 733.8 | 0.0135 |

## Conclusion

By the hydrothermal synthesis method, after reaction under the condition of 120 °C for 12 hours, the synthesized Cu-BTC particles have a regular octahedral structure, and the surface of the particles is approximately regular triangle shape. At the same time, the pore structure is regularly arranged and the chemical properties are stable. By electrospinning method, Cu-BTC particles are used to prepare Cu-BTC/PAN film. Compared with PAN fibers,

Cu-BTC/PAN fibers have smooth surface and uniform thickness, and the Cu-BTC/PAN membrane has extremely excellent air filtration performance, 8.5 times better than the PAN membrane.

## References

[1] Fisher, J. E., *et al*., Physical Activity, Air Pollution and the Risk of Asthma and Chronic Obstructive Pulmonary Disease, *American Journal of Respiratory and Critical Care Medicine*, *194* (2016), 7, pp. 855-865
[2] Thavasi, V., *et al*., Electrospun Nanofibers in Energy and Environmental Applications, *Energy and Environmental Science*, *1* (2008), 2, pp. 205-221
[3] Lee, E. S., *et al*., Evaluation of a High Efficiency Cabin Air (HECA) Filtration System for Reducing Particulate Pollutants Inside School Buses, *Environmental Science and Technology*, *49* (2015), 6, pp. 3358-3365
[4] Novoselov, K. S., *et al*., The 2-D Gas of Massless Dirac Fermions in Graphene, *Nature*, *438* (2005), 7065, pp. 197-200
[5] Novoselov, K. S., *et al*., Unconventional Quantum Hall effect and Berry's Phase of 2π in Bilayer Graphene, *Nature Physics*, *2* (2006), 3, pp. 177-180
[6] Li, X. X., He, J. H., Bubble Electrospinning with an Auxiliary Electrode and an Auxiliary Air-Flow, Recent Patents on Nanotechnology, *14* (2020), 1, pp. 42-45
[7] Li, Y., He, J.-H., Fabrication and Characterization of $ZrO_2$ Nanofibers by Critical Bubble Electrospinning for High-Temperature-Resistant Adsorption and Separation, *Adsorption Science and Technology*, *37* (2019), 5-6, pp. 425-437
[8] Cheng, T. T., *et al*., Effect of Surface-Active Agent on Bubble-Electrospun Polyacrylonitrile Nanofibers, *Thermal Science*, *23* (2019), 4, pp. 2481-2487
[9] Li, X. X., *et al.*, The Effect of Sonic Vibration on Electrospun Fiber Mats, *Journal of Low Frequency Noise Vibration and Active Control*, *38* (2019), 3-4, pp. 1246-1251
[10] He, C. H., et al., Taylor Series Solution for Fractal Bratu-Type Equation Arising in Electrospinning Process, *Fractals*, *28* (2020), 1, pp. 2189-2193
[11] Xu, G. J., *et al.*, Accurate Fabrication of Aligned Nanofibers Via a Double-Nozzle Near-Field Electrospinning, *Thermal Science*, *23* (2019), 4, pp. 2143-2150
[12] Yu, D. N, *et al*., Wetting and Supercontraction Properties of Spider-Based Nanofibers, *Thermal Science*, *23* (2019), 4, pp. 2189-2193
[13] Tian, D., *et al*., Sea-Silk Based Nanofibers and Their Diameter Prediction, *Thermal Science*, *23* (2019), 4, pp. 2253-2256
[14] He, C. H., *et al*., Effect of Concentration of Metal Inorganic Salt on Fiber Diameter in Electrospinning Process Mathematical Model and Experimental Verification, *Thermal Science*, *22* (2018), 6, pp. 2565-2570
[15] Li, X. X., et al., Thermal Property of Rock Powder-Based Nanofibers for High Temperature Filtration and Adsorption, *Thermal Science*, *23* (2019), 4, pp. 2501-2507
[16] He, J. H., Advances in Bubble Electrospinning, *Recent Patents on Nanotechnology*, *13* (2019), 3, pp. 162-163
[17] He, J. H., From Micro to Nanoand from Science to Technology: NanoAge Makes the Impossible Possible, *Micro and Nanosystems*, *12* (2020), 1, pp. 2-3
[18] Jin, C., *et al*., Deriving Carbon Atomic Chains from Graphene, *Physical Review Letters*, *102* (2009), 20, 205501
[19] Chui, S. S., A Chemically Functionalizable Nanoporous Material $[Cu_3(TMA)_2(H_2O)_3]_n$, *Science*, *283* (1999), 5405, pp. 1148-1150
[20] Kuppler, R. J., *et al*., Potential Applications of Metal-Organic Frameworks, *Coordination Chemistry Reviews*, *253* (2009), 23-24, pp. 3042-3066
[21] Hoskins, B. F., Robson, R., Infinite Polymeric Frameworks Consisting of 3-Dly Linked Rod-Like Segments, *Journal of the American Chemical Society*, *111* (1989), 15, pp. 5962-5964
[22] Liang, Z., *et al*., The $CO_2$ Adsorption-Based Separation by Metal Organic Framework (Cu-BTC) *vs*. Zeolite (13X), *Energy and Fuels*, *23* (2009), 5, pp. 2785-2789
[23] Luz, I., *et al*., Bridging Homogeneous and Heterogeneous Catalysis with MOF: Cu-MOF as Solid Catalysts for Three-Component Coupling and Cyclization Reactions for the Synthesis of Propargylamines, Indoles and Imidazopyridines, *Journal of Catalysis*, *285* (2012), 1, pp. 285-291

[24] Zhang, H., *et al*., A Thermodynamic Tank Model for Studying the Effect of Higher Hydrocarbons on Natural Gas Storage in Metal-Organic Frameworks, *Energy Environ. Sci*., *8* (2015), 5, pp. 1501-1510
[25] Davydovskaya, P., *et al*., Work Function Based Gas Sensing with Cu-BTC Metal-Organic Framework for Selective Aldehyde Detection, Sensors and Actuators B, *Chemical*, *187* (2013), Oct., pp. 142-146
[26] Li, R., *et al*., Integration of an Inorganic Semiconductor with a Metal-Organic Framework: A Platform for Enhanced Gaseous Photocatalytic Reactions, *Advanced Materials*, *26* (2014), 28, pp. 4783-4788
[27] Choi, K. M., *et al*., Supercapacitors of Nanocrystalline Metal-Organic Frameworks, *ACS Nano*, *8* (2014), 7, pp. 7451-7457
[28] Yang, C. F., *et al*., Existence Criterion of 3-D Regular Copper-1,3,5-Phenyltricarboxylate (Cu-BTC) Microparticles, *Journal of Donghua University*, *37* (2020), 2, pp. 116-120
[29] Yin, J., *et al*., Numerical Approach to High-throughput of Nanofibers by a Modified Bubble-Electrospinning, *Thermal Science*, *24* (2020), 4, pp. 2367-2375
[30] Ahmed, A., Xu, L., Numerical Analysis of the Electrospinning Process for Fabrication of Composite Fibers, *Thermal Science*, *24* (2020), 4, pp. 2377-2383
[31] Li, X. X., *et al*., Nanofibers Membrane for Detecting Heavy Metal Ions, *Thermal Science*, *24* (2020), 4, pp. 2463-2468
[32] Wu, Y. K., Liu, Y., Fractal-Like Multiple Jets in Electrospinning Process, *Thermal Science*, *24* (2020), 4, pp. 2499-2505
[33] He, C. H., *et al*., Taylor Series Solution for Fractal Bratu-Type Equation Arising in Electrospinning Process, *Fractal*s, *28* (2020), 1, 2050011
[34] He, J. H., On the Height of Taylor Cone in Electrospinning, *Results in Physics*, *17* (2020), June, 103096
[35] Zhang, H., *et al*., A Thermodynamic Tank Model for Studying the Effect of Higher Hydrocarbons on Natural Gas Storage in Metal-Organic Frameworks, *Energy and Environmental Science*, *8* (2015), 5, pp. 1501-1510
[36] Caudo, S., *et al*., The Cu-MOF: A New Highly Active Catalyst for WHPCO of Waste-Water from Agro-food Production, *Studies in Surface Science and Catalysis*, *170* (2007), Dec., pp. 2054-2059
[37] Szanyi, J., *et al.*, Well-Studied Cu-BTC Still Serves Surprises: Evidence for Facile $Cu^{2+}/Cu^{+}$ Interchange, Physical Chemistry Chemical Physics, *14* (2012), 13, 4383
[38] Ameloot, R., *et al*., Patterned Film Growth of Metal-Organic Frameworks Based on Galvanic Displacement, *Chemical Communications*, *46* (2010), 21, 3735
[39] Hartmann, M., *et al*., Adsorptive Separation of Isobutene and Isobutane on $Cu_3(BTC)_2$, *Langmuir*, *24* (2008), 16, pp. 8634-8642

Paper submitted: February 1, 2020
Paper revised: May 28, 2020
Paper accepted: May 28, 2020